Flow Past Rotating Cylinders: Effect of Eccentricity

S. Mittal
Associate Professor,
Department of Aerospace Engineering,
Indian Institute of Technology,
Kanpur, UP 208 016, India
e-mail: smittal@iitk.ac.in

Computational results are presented for flows past a translating and rotating circular cylinder. A stabilized finite element method is utilized to solve the incompressible Navier-Stokes equations in the primitive variables formulation. To validate the formulation and its implementation certain cases, for which the flow visualization and computational results have been reported by other researchers, are computed. Results are presented for Re=5, 200 and 3800 and rotation rate, (ratio of surface speed of cylinder to the freestream speed of flow), of 5. For all these cases the flow reaches a steady state. The values of lift coefficient observed for these flows exceed the limit on the maximum value of lift coefficient suggested by Goldstein based on intuitive arguments by Prandtl. These observations are in line with measurements reported, earlier, by other researchers via laboratory experiments. To investigate the stability of the computed steady-state solution, receptivity studies involving an eccentrically rotating cylinder are carried out. Computations are presented for flow past a rotating cylinder with wobble; the center of rotation of the cylinder does not match its geometric center. These computations are also important from the point of view that in a real situation it is almost certain that the rotating cylinder will be associated with a certain degree of wobble. In such cases the flow is unsteady and reaches a temporally periodic state. However, the mean values of the aerodynamic coefficients and the basic flow structure are still quite comparable to the case without any wobble. In this sense, it is found that the two-dimensional solution is stable to purely two-dimensional disturbances. [DOI: 10.1115/1.1380679]

1 Introduction

Flow past a spinning and translating cylinder has been a subject of numerous computational and experimental studies. Interest in this problem arises not only from the point of view of basic fluid mechanics but also from its applications to flow control. Tokumaru and Dimotakis [1,2] have demonstrated, via laboratory experiments, that a significant control on the structure of the wake can be achieved by subjecting the cylinder to rotary oscillations. Gad-el-Hak and Bushnel [3] review various techniques that are employed for separation control including the moving-surface boundary layer control (MSBC) in which rotating cylinder elements are employed to inject momentum into the already existing boundary layer.

Flow past an isolated rotating cylinder has been studied by various researchers in the past. The results of Prandtl and Reid from laboratory experiments have been reported by Goldstein [4]. These include the effect of the aspect ratio and end plates attached to the end of a cylinder that lead to an increase in the overall lift coefficient. Some of the later work on this flow problem include the development of the near-wake behind an impulsively started cylinder via flow visualization by Coutanceau and Menard [5]. The time evolution of the vortices in the near-wake for short time after the impulsive start comes out very clearly from their study. The highest Reynolds number in their study is less than 1000 and the rotation rate varies between 0 and 3.25. The nondimensional value of the rotation rate corresponds to the ratio of the speed on the surface of the cylinder and the freestream speed of flow. Badr and Dennis [6] gave numerical solutions for the viscous flow equations for small rotation rates 0.5, 1.0, and Re=200 and 500 in which comparisons with experiments of Coutanceau and Menard [5] have been made. Later, Badr et al. [7] presented computational and experimental results for Re=1000 and rotation rates between 0.5 and 3. Excellent match was obtained between the two except at high rotation rates where it is suspected that the experimental results show three-dimensional features. Computational results for the Re$=10^4$ flow were also presented.

Tokumaru and Dimotakis [2] measured the lift coefficient acting on rotating cylinders from their laboratory experiments. They have reported values of lift coefficient that exceed the limit set by Goldstein [4] based on the intuitive arguments given by Prandtl. According to Prandtl's arguments, the maximum value of the lift coefficient that can be achieved via Magnus effect is 4π ($\sim$12.6). For example, for Re$=3.8\times 10^3$ and $\alpha=10$ Tokumaru and Dimotakis [2] report an estimated lift coefficient that is more than 20 percent larger than this limit. This was observed for a cylinder with a span to diameter ratio of 18.7. Further, the trend of results that they have reported suggests that the value can be made larger for higher rotation rates and by taking cylinders of larger aspect ratio. They have suggested that perhaps it is the unsteady effects that weaken Prandtl's hypothesis and that the three-dimensional/end effects are responsible for lowering the value of lift coefficient that could be achieved in a purely two-dimensional flow. However, Chew et al. [8] have reported that their two-dimensional

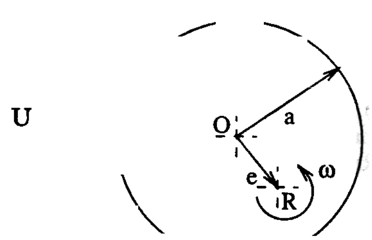

Fig. 1 Description of the eccentricity (e) of the rotating cylinder. The geometric center of the cylinder is at O while its axis of spin passes through R.

Contributed by the Applied Mechanics Division of THE AMERICAN SOCIETY OF MECHANICAL ENGINEERS for publication in the ASME JOURNAL OF APPLIED MECHANICS. Manuscript received by the ASME Applied Mechanics Division, Aug. 7, 2000; final revision, Nov. 29, 2000. Associate Editor: T. E. Tezduyar. Discussion on the paper should be addressed to the Editor, Prof. Lewis T. Wheeler, Department of Mechanical Engineering, University of Houston, Houston, TX 77204-4792, and will be accepted until four months after final publication of the paper itself in the ASME JOURNAL OF APPLIED MECHANICS.

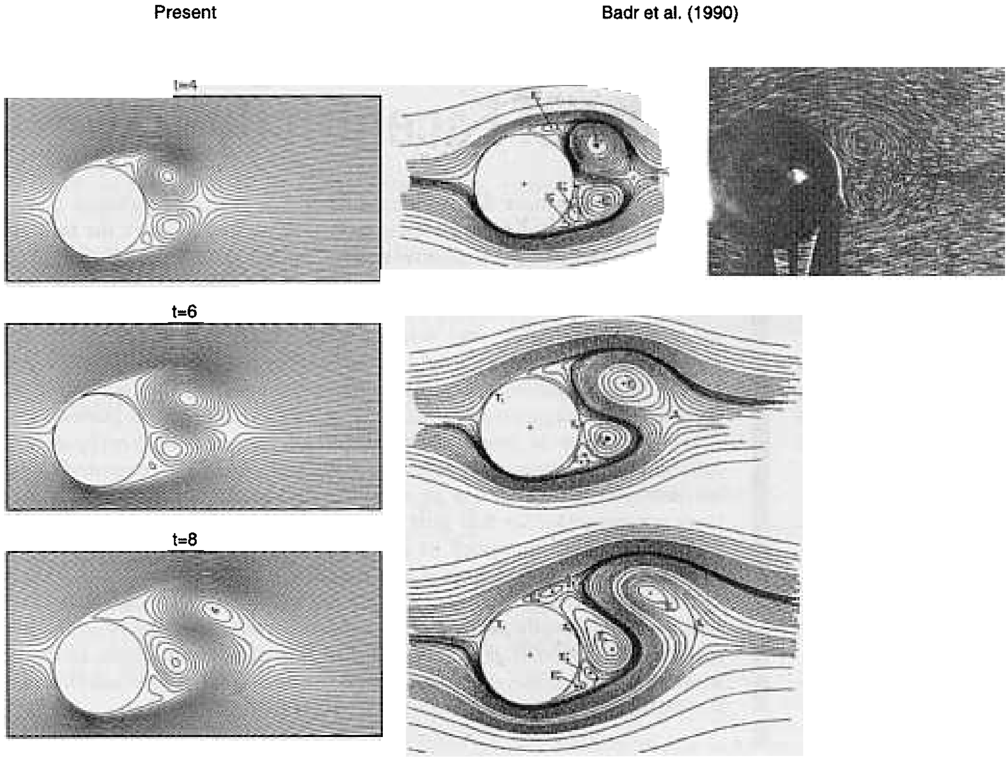

Fig. 2 Re$=10^3$, $\alpha=0.5$ flow past a rotating cylinder: comparison of the instantaneous streamline patterns at various time instants from the present computations and those from Badr et al. [8]

computations are in agreement with Prandtl's postulate. They find that for Re$=1000$, the estimated mean lift coefficient approaches asymptotic values with increase in α. At $\alpha=6$ they predict a mean lift coefficient of 9.1. The magnitude of lift generated by a cylinder for higher rates of rotation is an issue that remains unresolved even to this date. In this sense, the present work assumes significance in contributing to the efforts of resolving the issue regarding the limit on maximum lift that is possible via Magnus effect.

The objective of the present work is to investigate flows past spinning and translating cylinder at high rotation rates and determine the correctness of the limit on maximum lift set due to arguments by Prandtl. Stabilized space-time formulations for incompressible flows that have, earlier, been applied to a variety of flow problems are utilized for computations. First, the formulation and its implementation are validated for flows involving rotating cylinders by carrying out computations for Re$=1000$ and rotation rates of 0.5 and 2.0. The results are in excellent agreement with the flow visualizations and computational studies carried out by other researchers, earlier. For rotation rate of 3.0 the results from present computations match very well with other computed results, reported earlier. However, the experimental results show certain differences as compared to the two-dimensional computations for larger times. This may be attributed to the three-dimensional nature of the flow. At high rotation rates it is seen that the lift for purely two-dimensional setup can be very large. The values of the lift coefficient obtained in the present work exceed the maximum limit based on the arguments of Prandtl. The observations are consistent with the result of Tokumaru and Dimotakis [2]. For the Reynolds number considered in the present study the flow achieves a steady state for a rotation rate of 5. The stability of this steady-state solution, at least to two-dimensional disturbances, is an issue that needs investigation. The result of this study will play a vital role in resolving the validity (or nonvalidity) of the Prandtl's limit on maximum lift coefficient.

Computations are carried out to study the receptivity of the flow for eccentric/wobbly rotation of the cylinder. The center of rotation of the cylinder is slightly displaced with respect to the geometric center. This introduces an unsteadiness in the flow via the motion of the cylinder. The results are compared with those for noneccentrically rotating cylinder. Computations for various values of eccentricities show that the basic flow structure and the mean value of the lift coefficient do not differ much from that for the basic solution. This reflects the stability of the purely two-dimensional flow to two-dimensional disturbances. This study also brings out the effect of the eccentricity of the cylinder on the flow and the time histories of the aerodynamic coefficients.

The outline of the rest of the article is as follows. We begin by reviewing the governing equations for incompressible fluid flow in Section 2. The SUPG (streamline-upward/Petrov-Galerkin) and PSPG (pressure-stabilizing/Petrov-Galerkin) stabilization technique ([9–11]) is employed to stabilize our computations against spurious numerical oscillations and to enable us to use equal-order-interpolation velocity-pressure elements. Computations for the eccentrically rotating cylinders have been carried out with the DSD/SST (deforming-spatial-domain/stabilized-space-time) formulation ([12,13]). Section 3 describes the finite element formulations. In Section 4 computational results for flows involving rotating cylinder are presented and discussed. In Section 5 the results are summarized and a few concluding remarks are made.

2 The Governing Equations

Let $\Omega_t \subset \mathbb{R}^{n_{sd}}$ and $(0,T)$ be the spatial and temporal domains, respectively, where n_{sd} is the number of space dimensions, and let Γ_t denote the boundary of Ω_t. The spatial and temporal coordinates are denoted by $\mathbf{x}$ and t. The Navier-Stokes equations governing incompressible fluid flow are

$$\rho\left(\frac{\partial \mathbf{u}}{\partial t}+\mathbf{u}\cdot\nabla\mathbf{u}-\mathbf{f}\right)-\nabla\cdot\boldsymbol{\sigma}=0 \quad \text{on} \quad \Omega_t \quad \text{for} \quad (0,T), \tag{1}$$

$$\nabla\cdot\mathbf{u}=0 \quad \text{on} \quad \Omega_t \quad \text{for} \quad (0,T) \tag{2}$$

Table 1 Re=5, 200 and 3800, α=5 flow past a rotating cylinder: steady-state values of the lift and drag coefficients

Case	Re	C_L	C_D	C_L/C_D
1	5	19.11	1.054	18.13
2	200	27.28	0.783	34.83
3	3800	25.94	0.709	36.60

Here ρ, $\mathbf{u}$, $\mathbf{f}$, and $\boldsymbol{\sigma}$ are the density, velocity, body force, and the stress tensor, respectively. The stress tensor is written as the sum of its isotropic and deviatoric parts:

$$\boldsymbol{\sigma}=-p\mathbf{I}+\mathbf{T},\quad \mathbf{T}=2\mu\boldsymbol{\varepsilon}(\mathbf{u})\quad \boldsymbol{\varepsilon}(\mathbf{u})=\frac{1}{2}((\nabla\mathbf{u})+(\nabla\mathbf{u})^T),\tag{3}$$

where p and μ are the pressure and viscosity and $\mathbf{I}$ is the identity tensor. Both the Dirichlet and Neumann-type boundary conditions are accounted for, represented as

$$\mathbf{u}=\mathbf{g}\qquad (\Gamma_t)_g\qquad \mathbf{n}\cdot\boldsymbol{\sigma}=\mathbf{h}\quad \text{on}\quad (\Gamma_t)_h\tag{4}$$

where $(\Gamma_t)_g$ and $(\Gamma_t)_h$ are the complementary subsets of the boundary Γ_t and $\mathbf{n}$ is its unit normal vector. The initial condition on the velocity is specified on Ω_t at $t=0$:

$$\mathbf{u}(\mathbf{x},0)=\mathbf{u}_0\quad \text{on}\quad \Omega_t\tag{5}$$

where $\mathbf{u}_0$ is divergence free. The force coefficients are computed by carrying an integration, that involves the pressure and viscous stresses, around the circumference of the cylinder:

$$C_D=\frac{1}{1/2)\rho_\infty U_\infty^2 2a}\int(\boldsymbol{\sigma}\mathbf{n})\cdot\mathbf{n}_x d\Gamma\tag{6}$$

$$C_L=\frac{1}{1/2)\rho_\infty U_\infty^2 2a}\int(\boldsymbol{\sigma}\mathbf{n})\cdot\mathbf{n}_y d\Gamma\tag{7}$$

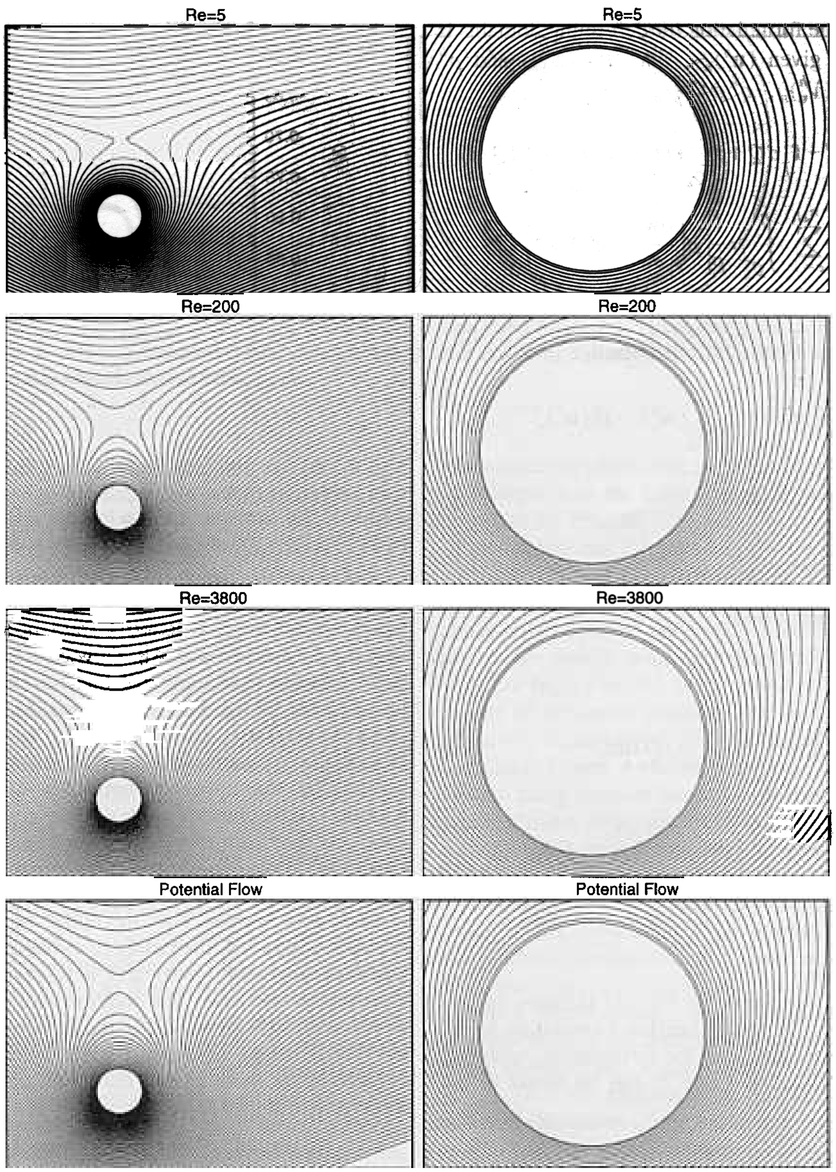

Fig. 3 Re=5,200 and 3800, α=5.0 flow past a rotating cylinder: streamlines for the steady-state solution. The potential flow solution is also shown for comparison.

Here, $\mathbf{n}_x$ and $\mathbf{n}_y$ are the Cartesian components of the unit vector $\mathbf{n}$ that is normal to the cylinder boundary Γ_{cyl} and a is the radius of the cylinder.

3 Finite Element Formulation

To accommodate the motion of the cylinder and the deformation of the mesh, a formulation that can handle moving boundaries and interfaces is employed. In order to construct the finite element function spaces for the space-time method, we partition the time interval $(0,T)$ into subintervals $I_n=(t_n,t_{n+1})$, where t_n and t_{n+1} belong to an ordered series of time levels: $0=t_0<t_1<\cdots<t_N=T$. Let $\Omega_n=\Omega_{t_n}$ and $\Gamma_n=\Gamma_{t_n}$. We define the space-time slab Q_n as the domain enclosed by the surfaces Ω_n, Ω_{n+1}, and P_n, where P_n is the surface described by the boundary Γ_t as t traverses I_n. As is the case with Γ_t, the surface P_n is decomposed into $(P_n)_g$ and $(P_n)_h$ with respect to the type of boundary condition (Dirichlet or Neumann) being imposed. For each space-time slab we define the corresponding finite element function spaces: $(\mathcal{S}^h_{\mathbf{u}})_n$, $(\mathcal{V}^h_{\mathbf{u}})_n$, $(\mathcal{S}^h_p)_n$, and $(\mathcal{V}^h_p)_n$. Over the element domain, this space is formed by using first-order polynomials in space and time. Globally, the interpolation functions are continuous in space but discontinuous in time.

The stabilized space-time formulation for deforming domains is then written as follows: given $(\mathbf{u}^h)_{n^-}$, find $\mathbf{u}^h\in(\mathcal{S}^h_{\mathbf{u}})_n$ and $p^h\in(\mathcal{S}^h_p)_n$ such that $\forall\mathbf{w}^h\in(\mathcal{V}^h_{\mathbf{u}})_n$, $q^h\in(\mathcal{V}^h_p)_n$,

$$\begin{aligned}&\int_{Q_n}\mathbf{w}^h\cdot\rho\left(\frac{\partial\mathbf{u}^h}{\partial t}+\mathbf{u}^h\cdot\nabla\mathbf{u}^h-\mathbf{f}\right)dQ+\int_{Q_n}\varepsilon(\mathbf{w}^h):\sigma(p^h,\mathbf{u}^h)dQ\\&+\int_{Q_n}q^h\nabla\cdot\mathbf{u}^h dQ+\sum_{e=1}^{n_{el}}\int_{Q_n^e}\tau\frac{1}{\rho}\left[\rho\left(\frac{\partial\mathbf{w}^h}{\partial t}+\mathbf{u}^h\cdot\nabla\mathbf{w}^h\right)\right.\\&\left.-\nabla\cdot\sigma(q^h,\mathbf{w}^h)\right]\cdot\left[\rho\left(\frac{\partial\mathbf{u}^h}{\partial t}+\mathbf{u}^h\cdot\nabla\mathbf{u}^h-\mathbf{f}\right)-\nabla\cdot\sigma(p^h,\mathbf{u}^h)\right]dQ\\&+\sum_{e=1}^{n_{el}}\int_{Q_n^e}\delta\nabla\cdot\mathbf{w}^h\rho\nabla\cdot\mathbf{u}^h dQ+\int_{\Omega_n}(\mathbf{w}^h)_n^+\cdot\rho((\mathbf{u}^h)_n^+\\&-(\mathbf{u}^h)_n^-)d\Omega=\int_{(P_n)_h}\mathbf{w}^h\cdot\mathbf{h}^h dP.\end{aligned}\tag{8}$$

This process is applied sequentially to all the space-time slabs $Q_0,Q_1,\ldots Q_{n-1}$. In the variational formulation given by Eq. (8), the following notation is being used:

$$(\mathbf{u}^h)_n^{\pm}=\lim_{\varepsilon\to 0}\mathbf{u}(t_n\pm\varepsilon),\tag{9}$$

$$\int_{Q_n}(\ldots)dQ=\int_{I_n}\int_{\Omega_n}(\ldots)d\Omega dt,\tag{10}$$

$$\int_{P_n}(\ldots)dP=\int_{I_n}\int_{\Gamma_n}(\ldots)d\Gamma dt.\tag{11}$$

The computations start with

$$(\mathbf{u}^h)_0^-=\mathbf{u}_0,\tag{12}$$

where $\mathbf{u}_0$ is divergence free.

The variational formulation given by Eq. (8) includes certain stabilization terms added to the basic Galerkin formulation to enhance its numerical stability. Details on the formulation, including the definitions of the coefficients τ and δ, can be found in the references [9,12,13].

4 Numerical Simulations

Flow past a cylinder spinning about its own axis has been studied by various researchers in the past. Most of the computations reported earlier, for this flow problem, have been carried out using the vorticity/stream-function formulations [7,8] or the vorticity/velocity formulations ([14]). However, the present effort employs finite element formulation of the Navier-Stokes equations in the primitive variables. The cylinder resides in a rectangular domain and a flow velocity corresponding to the rotation rate, α is specified on the cylinder surface. Freestream value is assigned for the velocity at the upstream boundary while at the downstream boundary, a Neumann-type boundary condition for the velocity is specified that corresponds to zero viscous stress vector. On the upper and lower boundaries, the component of velocity normal to and the component of stress vector along these boundaries is prescribed zero value. The Reynolds number is defined as $\mathrm{Re}=2Ua/\nu$ where a is the radius of cylinder, U the freestream speed (after an impulsive start) and ν is the coefficient of kinematic viscosity of the fluid. The rotation rate of the cylinder is nondimensionalized with respect to the freestream speed and is given as $\alpha=a\omega/U$ where ω is the angular velocity of the cylinder. the cylinder spins about an axis that is off-centered and is located at a distance e from its geometric center as shown in Fig. 1.

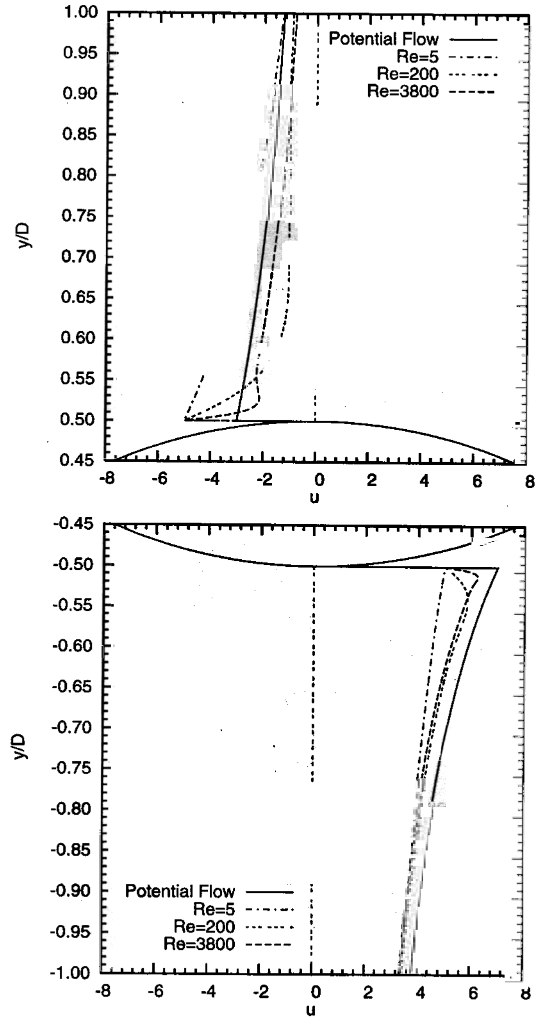

Fig. 4 Re=5, 200 and 3800, α=5.0 flow past a rotating cylinder: variation of the x-component of velocity along normals located at the uppermost and lowest points on the cylinder. The potential flow solution is also shown for comparison.

4.1 Re=1000, $e=0$, α=0.5, 2.0, 3.0. To establish confidence in the formulation and its implementation, the computed results for various rotation rates are compared with numerical and experimental results, reported earlier. The eccentricity is 0 in these cases; the cylinder spins about its own axis. Figure 2 shows the

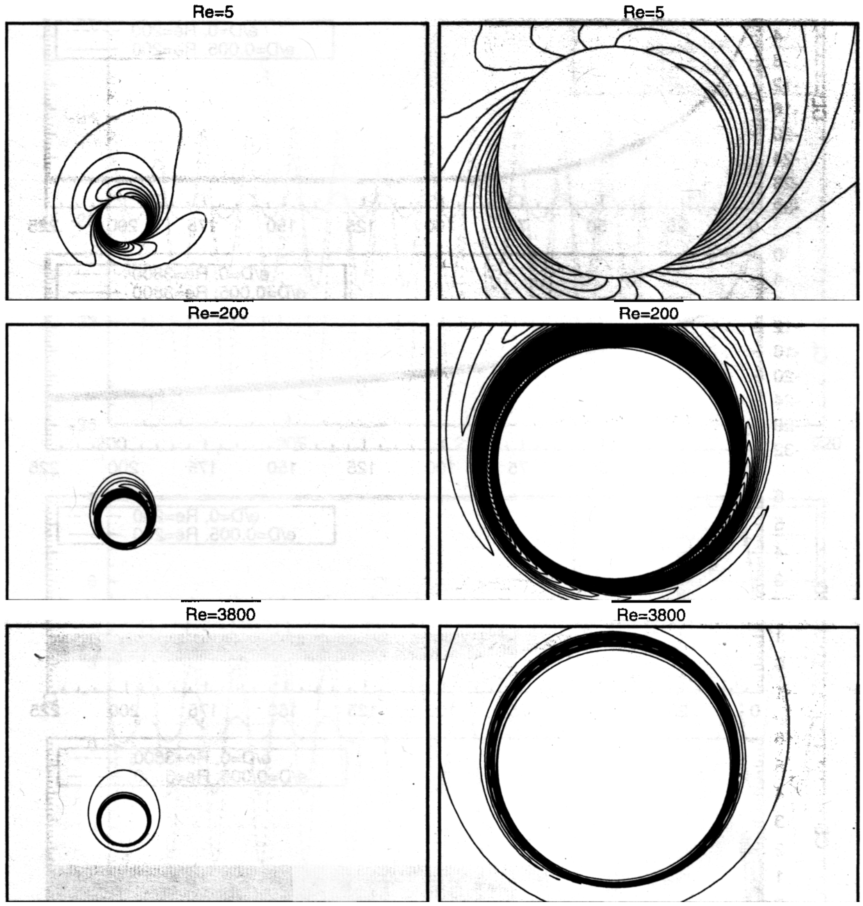

Fig. 5 Re=5, 200 and 3800, α=5.0 flow past a rotating cylinder: vorticity field for the steady-state solution

results for the computation of Re$=10^3$ flow past a cylinder with $\alpha=0.5$ with an impulsive start. Also shown in the figure are the computational and experimental results from Badr et al. [7]. The computations have been carried out with a mesh containing 12,408 nodes and 12,176 quadrilateral elements. All the external boundaries are located at eight cylinder diameters from the cylinder center. The time-step for the computations is 0.01. It can be observed from the figure that the present computations reproduce all the essential features of the flow and their time evolution. The instantaneous streamlines, shown in the figure, have been derived from the computed velocity field via a least squares procedure. The results for Re$=1000$ and $\alpha=2$, 3 (not shown here) also result in excellent agreement.

4.2 Re=5, 200 and 3800, $e=0$, $\alpha=5.0$. The next set of results are for long time behavior of the flow for rotation rate $\alpha=5$, and various Reynolds numbers. During the entire simulation for Re$=5$ only one clockwise vortex (the startup vortex) is shed from the rotating cylinder. A set of closed streamlines form around the rotating cylinder. In this computation, the finite element mesh consists of 12,678 nodes and 12,420 four-noded quadrilateral elements. The mesh is fine enough to resolve the boundary layer and other flow features, adequately, for this low Reynolds number. The external boundaries are located at 25 cylinder diameters from the center of the cylinder. Computations with a domain with the boundaries located at 20 cylinder diameters from the cylinder result in an almost indistinguishable solution. For more details on the effect of placement of lateral boundaries on the computed flow past a cylinder at Re$=100$ the reader may refer to the article by Behr et al. [15]. The steady-state value of the lift and drag coefficients from the simulations are listed in Table 1. Note that the steady-state lift coefficient obtained from the present simulation is much larger than the limit set by Goldstein [4] based on intuitive arguments by Prandtl.

The streamlines for the steady-state solution for all the three Reynolds numbers are shown in Fig. 3. Also shown in the same figure are the streamlines for the potential flow solution. It is interesting to observe the effect of Reynolds number on the location of the saddle point compared to that for potential flows. While for higher Re the saddle point is located close to the vertical line of symmetry passing through the center of the cylinder, for Re$=5$, departure of the saddle point from this line is quite significant. Figure 4 shows the variation of the x component of velocity along normals located at the uppermost and lowest points on the cylinder. Also, shown in the same figure are the profiles for the potential flow solution. On the upper surface, the max speed (nondimensionalized with the freestream speed of the flow) for the potential flow is 3. For the viscous flow, the speed on the surface of the cylinder is 5. For Re$=5$, close to the cylinder, the speed decreases monotonically with height while it shows a nonmonotonic behavior for higher Reynolds numbers. For Re$=3800$, the speed first decreases, then increases and decreases again. On the lower surface the potential flow solution predicts a speed of 7 on the cylinder and it decreases, monotonically, away from the cylinder. For the viscous flow, this value is 5 and again a nonmonotonic variation of the speed distribution can be noticed. This results in an interesting pattern of the vorticity distribution as will be seen shortly.

The vorticity fields for various Reynolds numbers are shown in Fig. 5. The distribution of the vorticity on the surface of the cylinder for various Reynolds numbers shows very similar trends for

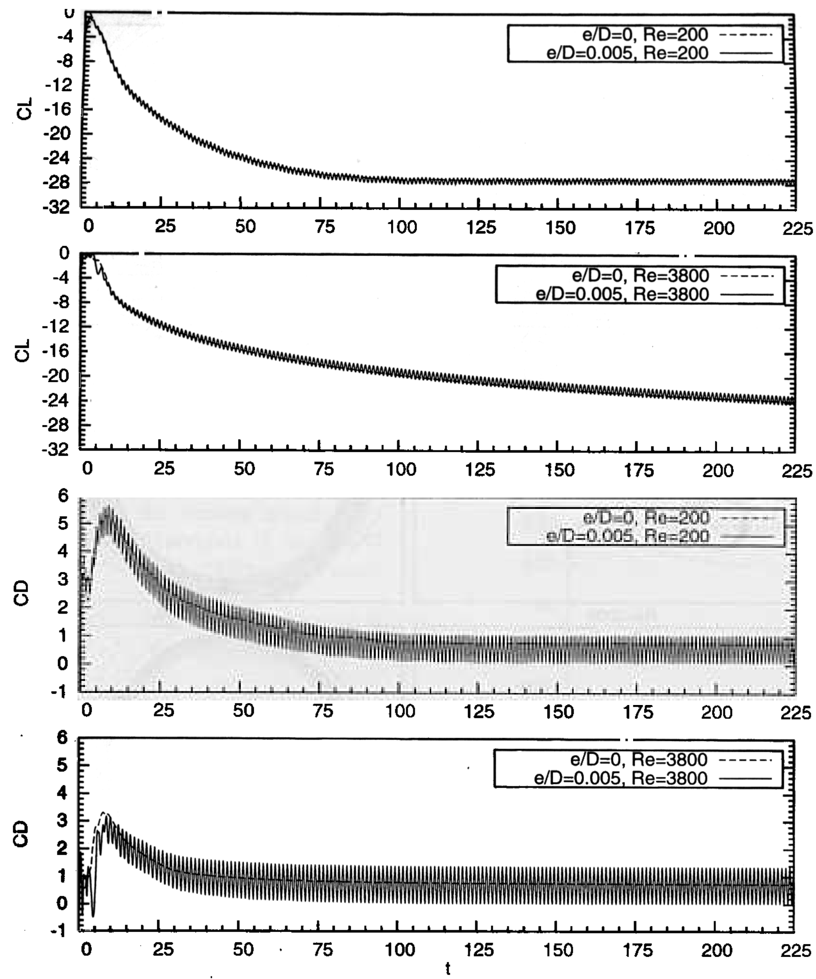

Fig. 6 Re=200, 3800, α=5.0, e=0.005 D flow past an eccentrically rotating cylinder: time-histories of the lift and drag coefficients

all the three cases. However, its magnitude is larger for higher Reynolds numbers. Since the cylinder is assigned a rotation in the counterclockwise direction, one might expect the surface vorticity to have the same sign all along the entire surface of the cylinder for the viscous flow solution. However, it is seen from the results that it changes sign twice. This suggests that the flow separates once and then reattaches on the cylinder surface. Notice, from the plot from stream function, that there is a set of closed streamlines near the cylinder. Also, the *Magnus effect* causes the pressure on the lower side of the cylinder to be substantially lower than that on the upper side. As a result, the fluid particles, close to the cylinder surface, experience a favorable pressure gradient on the windward side and an adverse pressure gradient on the leeward side of the cylinder. These pressure gradients are responsible for the separation and reattachment of the flow close to the cylinder surface. This observation is consistent with that from Fig. 5 which shows that the iso-vorticity contours close to the cylinder appear as spirals. The variation of the vorticity near the lowest and uppermost regions close to the cylinder can also be correlated to the variation of the x-component of velocity as shown in Fig. 4. It is expected that for larger Reynolds numbers this effect will be much stronger and may lead to unsteadiness in the flow.

4.3 Re=200, e=0.005 D, 0.025 D, 0.05 D, α=5.0. It has been pointed out in the previous section that for purely two-dimensional flows the high rotation rate of the cylinder ($\alpha=5$) results in a steady-state flow and very large value of the lift coefficient. For such flows to exist in real situations, it is essential that they are stable. It is known from work of certain researchers, for example, Tokumaru and Dimotakis [2] that the three-dimensional effects result in a reduction of the lift values that can be achieved for two-dimensional flows. However, this issue has not been addressed yet in the context of a purely two-dimensional environment. Therefore, it is of interest to study the stability of the two-dimensional flows, to two-dimensional disturbances. One way of investigating the stability of a solution is by introducing a disturbance in the basic flow and then monitoring its time evolution. In the present work, the stability has been investigated via a receptivity study. Computations are carried out for an eccentrically rotating cylinder. It is hoped that the periodic forcing of the flow due to the eccentric/wobbly motion of the cylinder will excite any possible instabilities associated with the flow. As a result of this receptivity study, the final solution is expected to be unsteady. However, for a basic flow that is stable, it is expected that the time-averaged disturbed flow will not be too different from the basic solution. The computations are carried out using a space-time finite element method where the spatial domain is allowed to deform with respect to time. Calculations for $e=0$ with the space-time formulation yields results that are almost indistinguishable from those obtained in the previous section. This further adds to our confidence in the present results.

Various degrees of eccentricity are considered. In all cases, the computations begin with an impulsive start. The initial condition for the flow is the potential flow past a stationary cylinder. The geometric center is located at the rightmost location with respect

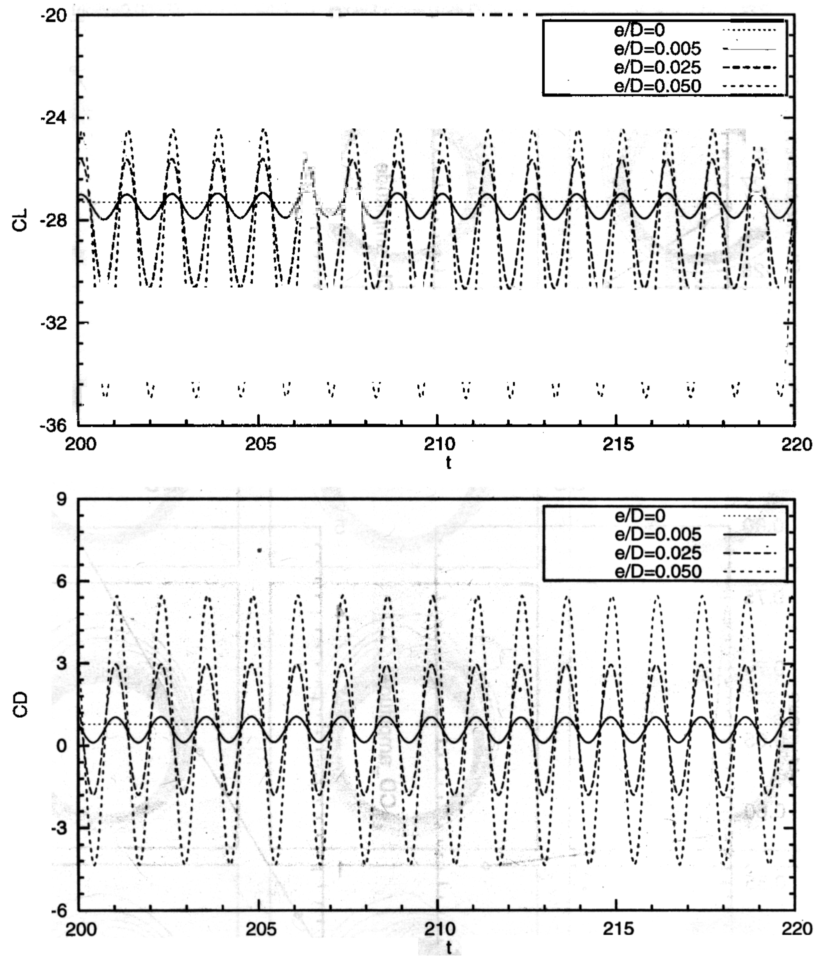

Fig. 7 Re=200, α=5.0 flow past an eccentrically rotating cylinder: close-up of the time histories of the lift and drag coefficients for various values of the eccentricity

to the center of rotation. With respect to Fig. 1 the coordinates of R relative to O are $(-e,0)$, at the start of computations.

Figure 6 shows the time histories of the lift and drag coefficients for the simulation with $e=0.005$ D. The aerodynamic coefficients show an oscillatory behavior. The frequency of oscillations is the same as that of the rotation of cylinder. It is interesting to note that the time histories of the mean values of the aerodynamic coefficients appear quite similar to the ones obtained for a cylinder with $e=0$. Similar observation is also made from the time histories of C_L and C_D for $e=0.025$ D and 0.05 D. A closeup of the time histories for various values of e are presented in Fig. 7. In all the cases, the frequency of the time variation of the aerodynamic coefficients is same and corresponds to the rotation rate of the cylinder. It can be observed that the amplitude of the unsteady force coefficients increase with eccentricity. However, the phase is same for all values of e. For values of e larger than 0.005 D, negative value of drag is observed during a certain part of each cycle of the cylinder motion. However, the mean drag over the entire cycle is always positive. A summary of the variation of the aerodynamic coefficients for various values of e is presented in Fig. 8. The magnitude of the mean lift coefficient increases with e. This could, perhaps, be explained by the increased strength of vortices for larger eccentricities of rotation. The mean drag coefficient shows a significant reduction for the case even with the lowest value of eccentricity ($e=0.005$ D) and then seems to change little with any further increase in eccentricity. However, the unsteady component of the drag coefficient shows a linear increase in amplitude with eccentricity. In all the cases the fully developed solution achieves a limit cycle and the basic flow structure remains the same. This suggests that the basic two-dimensional flow is quite stable, at least, to two-dimensional disturbances.

The vorticity fields at various instants during one cycle of cylinder rotation for the fully developed temporally periodic flows are shown in Fig. 9. From this figure it can be observed that the eccentric motion of the cylinder causes a vortex to be shed during each cycle of rotation of the cylinder. The size and strength of the vortex, that is shed, increase with increase in eccentricity of rotation. the dynamics of the vortex formation, its release and dissipation is quite clear from the figure for $e=0.05$ D. Somewhere between the second and third frames, a counterclockwise rotating vortex is shed from the cylinder. It travels around the periphery of the cylinder in the counterclockwise direction and is dissipated during the next cycle of rotation of the cylinder. These strong vortices also result in certain weaker induced vortices of opposite sign. The vortical activity due to the eccentricity of the rotation takes place very close to the cylinder, and its effect on the outer flow seems to be insignificant. These computations help us in concluding that the two-dimensional flow past the spinning cylinder, presented in the previous section, is stable to two-dimensional disturbances. Therefore, in a purely two-dimensional environment, the solutions presented in the earlier section can exist. This strengthens our point of view that the Prandtl's limit on the maximum lift coefficient generated by a spinning cylinder may not hold.

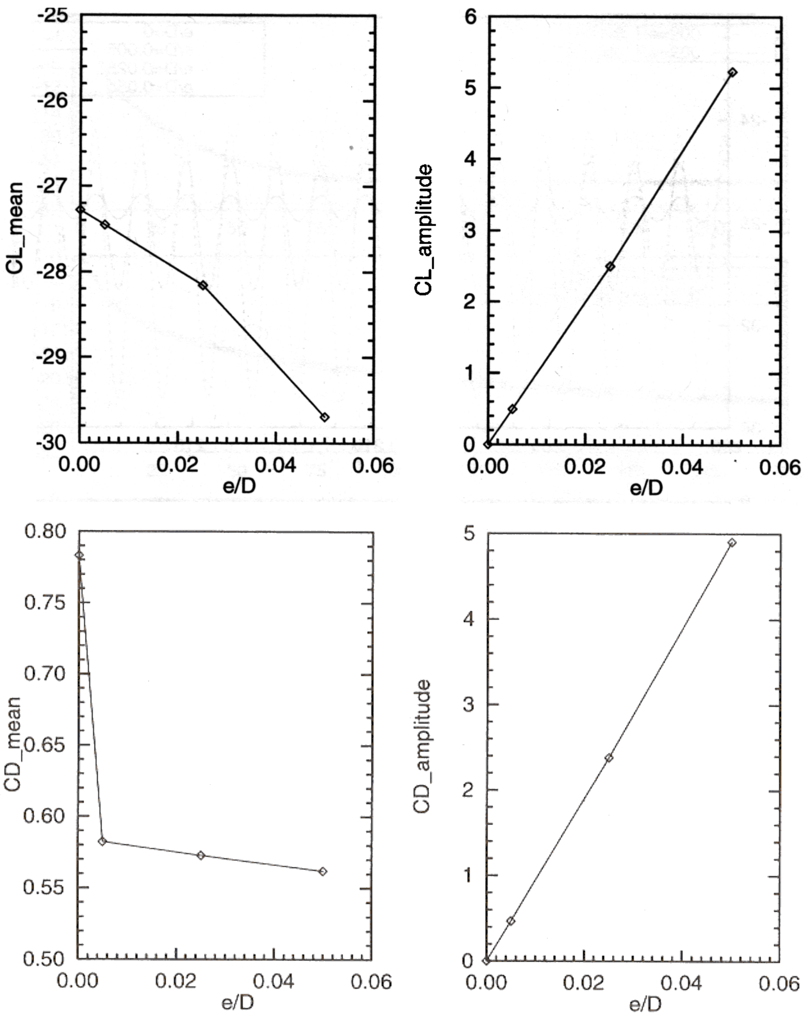

Fig. 8 Re=200, α=5.0 flow past an eccentrically rotating cylinder: summary of the aerodynamic coefficients for different values of the eccentricity

4.4 Re=3800, $e=0.005$ D, α=5.0. To determine the stability of the Re=3800 flow in a purely two-dimensional setup computations are carried out with $e=0.005$ D. Figure 6 shows the time histories of the aerodynamic coefficients. Also shown in the same figure are the time histories for the computations with $e=0$. As was observed for Re=200, the time evolution of the mean value of the aerodynamic coefficients follow the same trend as that for $e=0$. The eccentricity of rotation causes a sinusoidal variation in the temporal data and its frequency content is same as that of the rotation of cylinder. This shows that the eccentricity of the rotation of cylinder does not cause any significant change to the original steady solution. This reflects the stability of the two-dimensional solution, to purely two-dimensional disturbances. Figure 10 shows the vorticity, pressure and magnitude of velocity, close to the cylinder, at one time instant for the temporally periodic solution. On comparing this figure to Fig. 5 it can be observed that the effect of eccentricity in the rotational motion of the cylinder is restricted to a region very close to it.

To check the dependence of the solution on the spatial and temporal discretization, the solution was projected on a finer mesh with 26,830 nodes and 26,500 elements and the computations continued with a time step of 0.01. The aerodynamic coefficients for the new solution showed less than 0.1 percent difference in the mean values and less than 1.0 percent in the unsteady values.

5 Concluding Remarks

Flow past a rotating circular cylinder placed in a uniform stream has been studied numerically. A stabilized finite element method is utilized to solve the incompressible Navier-Stokes equations in the primitive variables formulation. Good agreement with some of the flow visualization and computational results from other researchers, reported earlier, is observed. Computations have been carried out for Re=5, 200, and 3800 and rotation rate, α, of 5. It is seen that for these parameters the flow achieves a steady-state and that the lift for purely two-dimensional setup can be very large. Both the semidiscrete and the space-time formulations have been utilized to compute the solution for α=5. They result in almost indistinguishable results adding further to the correctness of the present results. The flow close to the cylinder, for various Reynolds numbers, is compared to the potential flow solution. Interesting differences are observed in the various solutions. The vorticity distribution along the cylinder surface points to mild separation and reattachment of the flow. This is attributed to the adverse and favorable pressure gradients of the flow on the windward and leeward sides of the cylinder. It is expected that for even larger Reynolds numbers, the separation would become stronger and result in an unsteady flow. The values of the lift coefficient obtained in the present work exceed the maximum limit set by Goldstein based on the intuitive arguments

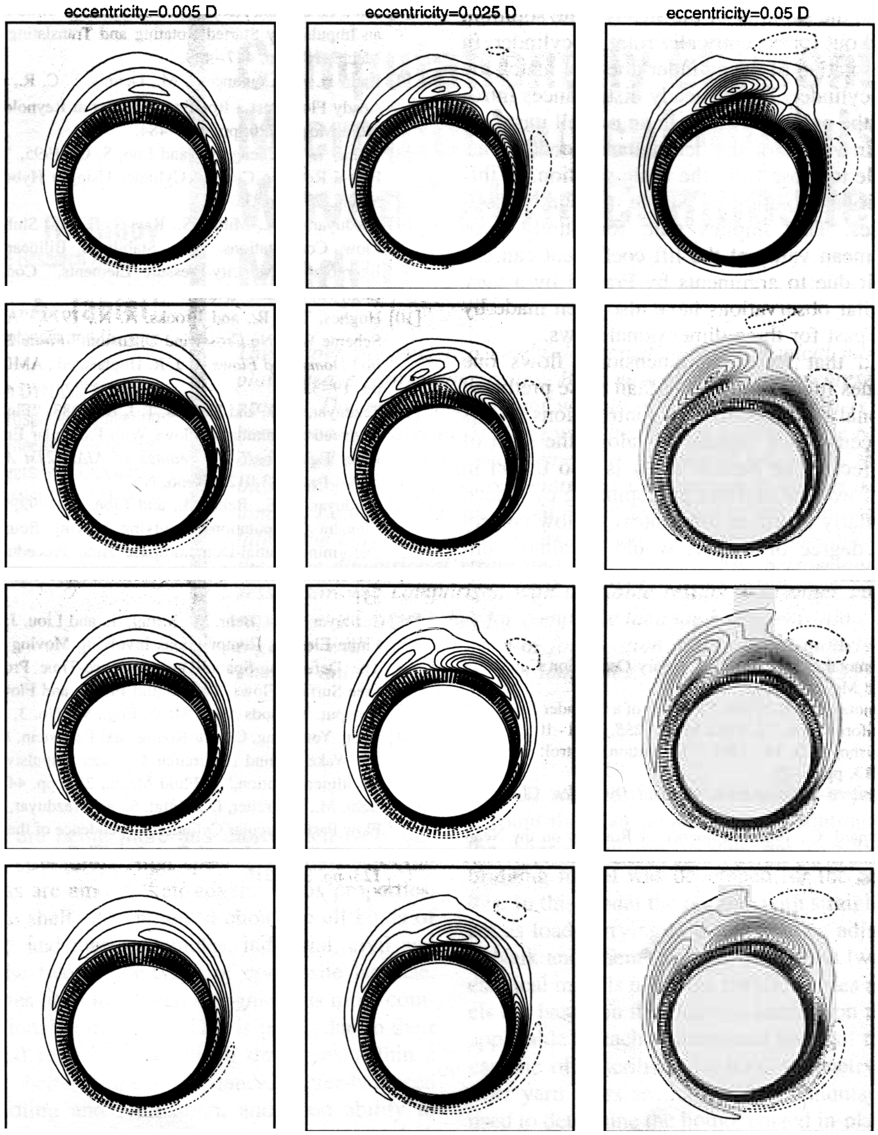

Fig. 9 Re=200, α=5.0 flow past an eccentrically rotating cylinder: vorticity field at four time instants during one period of rotation for the temporally periodic solution. The frames in the various rows from top to bottom correspond to the time instants when the geometric center of the cylinder is at its left-most, bottom-most, right-most, and top-most location, respectively, with respect to the center of rotation. The clockwise vorticity is shown in broken lines while the counterclockwise component is shown in solid lines.

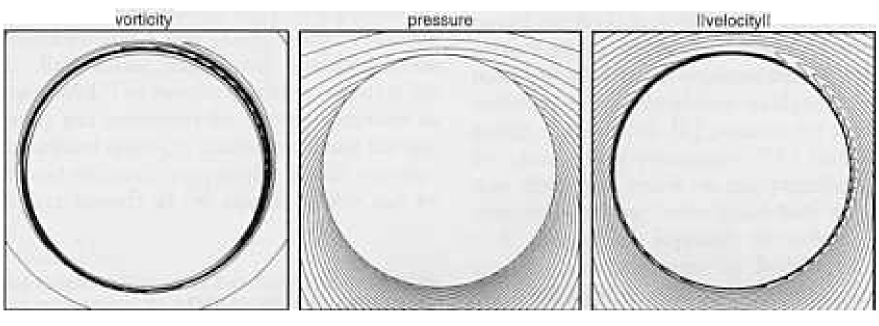

Fig. 10 Re=3800, α=5.0, e=0.005 D flow past an eccentrically rotating cylinder: vorticity, pressure, and magnitude of velocity fields for the temporally periodic solution when the geometric center of the cylinder is at its left-most location with respect to the center of rotation

by Prandtl. To investigate the stability of the steady-state solution, computations are carried out for eccentrically rotating cylinder. In this set-up the center of rotation of the cylinder does not match the geometric center of the cylinder. The unsteady disturbances introduced by the motion of the cylinder results in an overall unsteady flow. However, the mean values of the aerodynamic coefficients are still quite comparable to those from the basic solution. In this sense, the two-dimensional solution is stable to purely two-dimensional disturbances. This implies that, for purely two-dimensional flows, the mean value of the lift coefficient can exceed the maximum limit due to arguments by Prandtl by a very significant amount. Similar observations have also been made by other researchers in the past for three-dimensional flows.

It is being suggested that for three-dimensional flows one should expect lower values for lift coefficient than those predicted by purely two-dimensional simulations. The contributions to this loss of lift come from centrifugal instabilities along the span of the cylinder and end effects. The present study is also useful in establishing the effect of *wobble* in flows past spinning cylinders. These results are particularly useful in the context of flow control devices where a slight degree of wobble would be almost unavoidable in real situations.

References

[1] Tokumaru, P. T., and Dimotakis, P. E., 1991, "Rotary Oscillation Control of Cylinder Wake," J. Fluid Mech., **224**, pp. 77–90.

[2] Tokumaru, P. T., and Dimotakis, P. E., 1993, "The Lift of a Cylinder Executing Rotary Motions in a Uniform Flow," J. Fluid Mech., **255**, pp. 1–10.

[3] Gad-el-Hak, M., and Bushnell, D. M., 1991, "Separation Control: Review," ASME J. Fluids Eng., **113**, pp. 5–29.

[4] Goldstein, S., 1938, *Modern Developments in Fluid Dynamics,* Clarendon Press, Oxford, U.K.

[5] Coutanceau, M. and Menard, C., 1985, "Influence of Rotation on the Near-Wake Development Behind an Impulsively Started Circular Cylinder," J. Fluid Mech., **158**, pp. 399–446.

[6] Badr, H. M., and Dennis, S. C. R., 1985, "Time-Dependent Viscous Flow Past an Impulsively Started Rotating and Translating Circular Cylinder," J. Fluid Mech., **158**, pp. 447–488.

[7] Badr, H. M., Coutanceau, M., Dennis, S. C. R., and Menard, C., 1990, "Unsteady Flow Past a Rotating Cylinder at Reynolds Numbers 10^3 and 10^4," J. Fluid Mech., **220**, pp. 459–484.

[8] Chew, Y. T., Cheng, M., and Luo, S. C., 1995, "A Numerical Study of Flow Past a Rotating Circular Cylinder Using a Hybrid Vortex Scheme," J. Fluid Mech., **299**, pp. 35–71.

[9] Tezduyar, T. E., Mittal, S., Ray, S. E., and Shih, R., 1992, "Incompressible Flow Computations With Stabilized Bilinear and Linear Equal-Order-Interpolation Velocity-Pressure Elements," Comput. Methods Appl. Mech. Eng., **95**, pp. 221–242.

[10] Hughes, T. J. R., and Brooks, A. N., 1979, "A Multi-Dimensional Upwind Scheme With No Crosswind Diffusion," *Finite Element Methods for Convection Dominated Flows,* T. J. R. Hughes, ed., AMD-Vol. 34, ASME, New York, pp. 19–35.

[11] Tezduyar, T. E., and Hughes, T. J. R., 1983, "Finite Element Formulations for Convective Dominated Flows With Particular Emphasis on the Compressible Euler Equations," *Proceedings of AIAA 21st Aerospace Sciences Meeting,* AIAA Paper 83-0125, Reno, NV.

[12] Tezduyar, T. E., Behr, M., and Liou, J., 1992, "A New Strategy for Finite Element Computations Involving Moving Boundaries and Interfaces—The Deforming-Spatial-Domain/Space-Time Procedure: I. The Concept and the Preliminary Tests," Comput. Methods Appl. Mech. Eng., **94**, No. 3, pp. 339–351.

[13] Tezduyar, T. E., Behr, M., Mittal, S., and Liou, J., 1992, "A New Strategy for Finite Element Computations Involving Moving Boundaries and Interfaces—The Deforming-Spatial-Domain/Space-Time Procedure: II. Computation of Free-Surface Flows, Two-Liquid Flows, and Flows With Drifting Cylinders," Comput. Methods Appl. Mech. Eng., **94**, No. 3, pp. 353–371.

[14] Chen, Yen-Ming, Ou, Yu-Roung, and Pearlstein, A. J., 1993, "Development of the Wake Behind A Circular Cylinder Impulsively Started Into Rotary and Rectilinear Motion," J. Fluid Mech., **253**, pp. 449–484.

[15] Behr, M., Hastreiter, D., Mittal, S., and Tezduyar, T. E., 1995, "Incompressible Flow Past a Circular Cylinder: Dependence of the Computed Flow Field on the Location of the Lateral Boundaries," Comput. Methods Appl. Mech. Eng., **123**, pp. 309–316.